Journal of
Water & Climate Change

Precipitation barycenter and relationship to the spatial distribution of station networks on the Huang-Huai-Hai Plain, China

Minhua Ling[a,b,c,*], Hongbao Han[a], Lili Yu[d] and Shinan Tang[d]

[a] School of Water Conservancy Engineering, Zhengzhou University, Zhengzhou 450001, China
[b] Yellow River Institute for Ecological Protection & Regional Coordinated Development, Zhengzhou University, Zhengzhou 450001, China
[c] Zhengzhou Key Laboratory of Water Resource and Environment, Zhengzhou University, Zhengzhou 450001, China
[d] General Institute of Water Conservancy and Hydropower Planning and Design, Ministry of Water Resources, Beijing 100032, China
*Corresponding author. E-mail: 1044181701@qq.com

ABSTRACT

A precipitation barycenter reflects the overall spatial distribution and long-term evolution of regional precipitation. Understanding the changes in precipitation barycenter has significant implications for drought management, flood control, and water resource management. This paper analyzed the distribution and transfer of monthly, interannual, and interdecadal precipitation barycenter on the Huang-Huai-Hai Plain ('3H' Plain). We also discussed the influence of the station network spatial distribution on the changes in precipitation barycenter. The results were as follows: (1) The trajectory of the monthly precipitation barycenter on the '3H' Plain was generally '8'-shaped. The rainy and dry season precipitation barycenters were located in the upper and lower parts of the '8'-shaped, respectively. (2) In the past 60 years, the interannual precipitation barycenter had a trend of moving southwest, but the trend was not apparent. (3) Station network density and uniformity dominated the changes in precipitation barycenter, showing positive correlations. When the station network density was large and exceeded a certain range, the influence of station network density on the changes in precipitation barycenter decreased.

Key words: canonical correlation analysis, Huang-Huai-Hai Plain, precipitation barycenter, station network distribution

HIGHLIGHTS

- Precipitation barycenters of the Huang-Huai-Hai Plain.
- The monthly precipitation barycenter generally follows an '8'-shaped movement track.
- The interannual precipitation barycenter tended to move southwest in the past 60 years.
- Precipitation barycenter relationship with the spatial distribution of station network.

1. INTRODUCTION

In recent years, as a global environmental issue, climate change has received widespread attention from society (Fu *et al.* 2016). The '3H' Plain is one of the climatic sensitive areas in China (Rong & Luo 2009), which belongs to the warm temperate monsoon climate. In recent decades, the spatial–temporal distributions of precipitation have been highly uneven, and droughts and floods have occurred frequently on the '3H' Plain (Zhang *et al.* 2015). At present, research on the spatial–temporal variation characteristics of precipitation on the '3H' Plain mainly focuses on extreme precipitation. Li *et al.* (2018) analyzed the temporal variations and spatial distributions of annual average precipitation and extreme precipitation from the perspectives of time and space on the '3H' Plain. They found that the distribution of the extreme precipitation index is similar to that of the annual precipitation index. Based on four extreme precipitation indices, Fang *et al.* (2018) analyzed the spatial–temporal variation characteristics of extreme precipitation on the '3H' Plain and its relationship with El Niño-Southern Oscillation (ENSO). However, less attention has been paid to the distribution and migration of the precipitation barycenter on the '3H' Plain.

The center of gravity originally belongs to the category of classical mechanics in physics. The basic meaning is that each part of an object is subjected to the point of gravity. In recent years, some scholars have extended the concept of the center of gravity to the field of meteorology. Liu *et al.* (2012) extended it as the center of gravity of rainfall erosivity and revealed the dynamic changes of concentrated distribution areas by studying the annual variation of rainfall erosivity in

southwest mountainous areas. Yao et al. (2021) extended it as the drought center of gravity and studied the aridification trend of the Huai River Basin through the trajectory of the drought center-of-gravity shift in the Huai River Basin. Chen et al. (2017), Zhao et al. (2018), and Qian (2011) extended it as the precipitation barycenter, analyzed the distribution and migration of the precipitation barycenter in different regions and different time scales, and revealed the degree of uneven spatial distribution of precipitation. A precipitation barycenter is defined as the point where the moment of precipitation on the spatial plane reaches equilibrium at a certain moment in the region (Sun et al. 2014). It can reflect the overall distribution of precipitation in the region (Luo et al. 2015). Its distribution trend reflects the dispersion, transfer, and dominant distribution of precipitation, which helps analyze the difference and balance of regional precipitation. The precipitation barycenter is calculated by weighting the precipitation based on the location information of the station. The spatial distribution of the station network (density and uniformity) directly affects the calculated result of the precipitation barycenter. However, current research on the relationship between the change in the precipitation barycenter and the spatial distribution of the station network is still lacking (Chen et al. 2017; Wu et al. 2017; Zhao et al. 2018).

Based on monthly precipitation data of the '3H' Plain from 1960 to 2019, this paper analyzed the distribution and transfer of monthly, interannual, and interdecadal precipitation barycenter in the study area and explored the relationship between changes in precipitation barycenter and the spatial distribution of the station network using the center-of-gravity model, standard deviation ellipse, canonical correlation analysis, and other methods. It is expected to provide references for agricultural production guarantees, disaster prevention and mitigation, and water resource allocation on the '3H' Plain.

2. DATA AND METHODS

2.1. Study region

The '3H' Plain is located south of Yanshan Mountains and north of Huai River (112°33′ ~ 120°17'E, 31°14' ~ 50°25'N), including Hebei, Henan, Shandong, Anhui, Jiangsu, Beijing, and Tianjin. As the economic and cultural center of China, it is the country's most populous plain, with a total population of 339 million in 2019. Its gross domestic product accounts for about a quarter of China. The '3H' Plain is one of the three great plains in China. It has a low and flat terrain with many rivers and lakes, most of which are below 50 meters above sea level. It is composed of alluvial plains of the Yellow River, Huai River, and Haihe River and some hilly mountains.

The '3H' Plain has a temperate monsoon climate and a subtropical monsoon climate, with obvious changes in the four seasons. The summer is affected by the southeast monsoon, high temperature, and rainy. The winter is affected by the northwest monsoon, cold, and dry. The average annual temperature and annual precipitation decrease from south to north as the latitude increases. The average annual precipitation on the '3H' Plain is 500–900 mm (Zhang et al. 2011). The precipitation distribution is extremely uneven, and about 80% of the precipitation is concentrated in summer. With the increase of sea surface temperature in the east of the equator and the central Pacific, the climate of the '3H' Plain shows a warming and drying trend (Fang et al. 2018; Wu et al. 2019). The '3H' Plain is an important food production base in China. The heat is suitable for two crops a year, and the main cultivation method is summer corn–winter wheat rotation (Yuan et al. 2019). It is the largest growing region of summer corn and winter wheat in China (Yang et al. 2015). The spatial distribution of meteorological stations on the '3H' Plain is shown in Figure 1.

2.2. Data sources

The monthly meteorological data of the 215 stations in the study area from 1960 to 2019 are from the China Meteorological Administration. The data have been quality-controlled and the quality is good. The data used in the study have no missing values.

2.3. Methods

2.3.1. Center-of-gravity model

As a physics concept, the center of gravity is derived from classical mechanics. The basic meaning refers to the point where each part of an object is affected by gravity. The concept of the center of gravity is extended to the regional center of gravity. The regional center of gravity is also called the spatial mean, which is the extension of the sample average in two-dimensional space. In the spatial dimension, the regional center of gravity reflects the degree of agreement between regional development indicators and centroid analysis, which is convenient to analyze the fluidity and aggregation of regional elements in space. In the time dimension, the dynamic change of regional center of gravity indicates the contrast and transfer of regional element
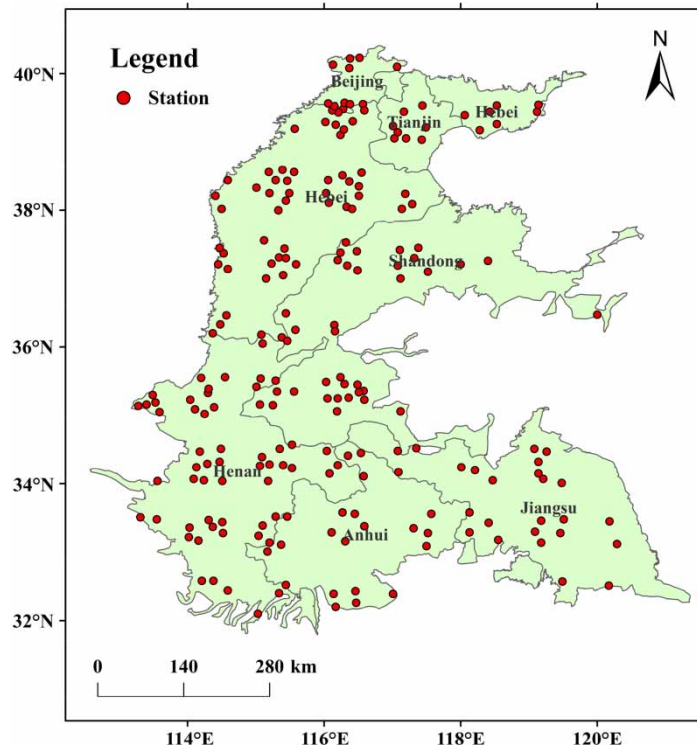
Figure 1 | Spatial distribution of meteorological stations on the '3H' Plain.

distribution, which is helpful to deepen the course, state, and trend of regional development. The regional center of gravity is usually calculated by the center-of-gravity model.

In recent years, the center-of-gravity model has been widely used in hydro-climate, ecological environment, economic, and social fields, including precipitation barycenter, pollution centers of gravity, and population centers of gravity (Gao & Liu 2006; Barmpas *et al.* 2017; Chen *et al.* 2017). To analyze the difference and balance of macro-precipitation on the '3H' Plain, the center-of-gravity model is introduced to analyze the accumulation, migration, and dominant distribution of precipitation. The precipitation barycenter of the area is calculated as follows:

$$X = \frac{\sum\limits_{i=1}^{n} x_i P_i}{\sum\limits_{i=1}^{n} P_i}, \quad Y = \frac{\sum\limits_{i=1}^{n} y_i P_i}{\sum\limits_{i=1}^{n} P_i} \tag{1}$$

where X and Y are the longitude and latitude coordinates of the precipitation barycenter; x_i and y_i are the longitude and latitude coordinates of the ith meteorological station; and P_i is the precipitation of the ith meteorological station.

2.3.2. Standard deviation ellipse

The standard deviation ellipse method was first proposed by Professor Lefever in 1926. This method can analyze the directionality and dispersion of the precipitation barycenter point group, and the result is an ellipse similar to its name. The major and minor axes of the ellipse indicate the direction and range of the point group distribution, respectively. The greater the difference between the major axis and the minor axis is (i.e., the greater the oblateness), the more obvious the directionality of the point group. Conversely, if the lengths of the major axis and the minor axis are more nearly equal, the directionality of the point group is less obvious. The longer the minor axis is, the greater the degree of dispersion of the point group. For a cluster of precipitation gravity points in a certain period, the standard deviation ellipse method can be used to analyze its directionality and distribution trend. The main calculation is described as follows (Yuan *et al.* 2020):

1. The center of the ellipse is determined:

$$\text{SDE}_x = \sqrt{\dfrac{\left[\sum\limits_{i=1}^{N}(X_i - \bar{X})^2\right]}{N}}, \ \ \text{SDE}_y = \sqrt{\dfrac{\left[\sum\limits_{i=1}^{N}(Y_i - \bar{Y})^2\right]}{N}},$$

$$\bar{X} = \dfrac{\left(\sum\limits_{i=1}^{N} X_i\right)}{N}, \ \ \bar{Y} = \dfrac{\left(\sum\limits_{i=1}^{N} Y_i\right)}{N} \tag{2}$$

2. The direction angle of the ellipse θ is determined:

$$\tan\theta = \dfrac{A+B}{C}, \ \ A = \left(\sum_{i=1}^{N}\tilde{X}_i^2 - \sum_{i=1}^{N}\tilde{Y}_i^2\right), \ \ B = \sqrt{\left(\sum_{i=1}^{N}\tilde{X}_i^2 - \sum_{i=1}^{N}\tilde{Y}_i^2\right)^2 + 4\left(\sum_{i=1}^{N}\tilde{X}_i\tilde{Y}_i\right)^2},$$

$$C = 2\sum_{i=1}^{N}\tilde{X}_i\tilde{Y}_i, \ \ \tilde{X}_i = X_i - \bar{X}, \ \ \tilde{Y}_i = Y_i - \bar{Y} \tag{3}$$

3. The lengths of the major and minor axes of the ellipse are determined:

$$\sigma_x = \sqrt{2}\sqrt{\dfrac{\sum\limits_{i=1}^{N}(\tilde{X}_i\cos\theta - \tilde{Y}_i\sin\theta)^2}{N}}, \ \ \sigma_y = \sqrt{2}\sqrt{\dfrac{\sum\limits_{i=1}^{N}(\tilde{X}_i\sin\theta + \tilde{Y}_i\cos\theta)^2}{N}} \tag{4}$$

where X_i and Y_i are the latitude and longitude coordinates of the precipitation barycenter; SDE_x and SDE_y are the center coordinates of the ellipse; $\tilde{X}_i$ and $\tilde{Y}_i$ are the differences between the arithmetic mean of the coordinates of the precipitation barycenter and the coordinates of the precipitation barycenter; σ_x and σ_y are the lengths of the major and minor axes of the ellipse, respectively; and N is the number of precipitation barycenters.

2.3.3. Canonical correlation analysis

In 1936, the mathematician Hotelling further promoted the concept of the correlation coefficient, studied the correlation between two sets of multidimensional variables, and proposed the canonical correlation analysis theory (Zhuang *et al.* 2020). The basic idea of canonical correlation analysis is dimensionality reduction (Robertson *et al.* 2001), which reduces the two sets of high-dimensional data to one-dimensional. We obtain a number of comprehensive indicators from each set of variables. These comprehensive indicators are linear combinations of variables. The purpose is to reduce the two sets of high-dimensional data to one-dimensional. The specific implementation process is to construct a covariance matrix, use the eigenvalues and eigenvectors of the matrix to obtain typical variables, and finally study the correlation. Canonical correlation represents the closeness between theoretical precipitation barycenter and approximate true precipitation barycenter in the spatial distribution of different station networks.

3. RESULTS AND DISCUSSION

3.1. Distribution characteristics of precipitation barycenters

We used the monthly average precipitation at 215 stations from 1960 to 2019, determining the monthly precipitation barycenter of the '3H' Plain. We plotted the migration track of the monthly precipitation barycenter on the '3H' Plain (Figure 2) and observed the movement direction and distance for each month relative to those of the previous month (Table 1). It can be seen from Figure 2 that the monthly precipitation barycenters on the '3H' Plain are mainly distributed in Jining city, Shandong Province, and Suzhou city, Anhui Province, which are between 34°15′ and 35°58′N and 116°10′ and 116°35′E. By the month, the precipitation barycenter in April moves the farthest. Compared to the barycenter in March, the precipitation barycenter moves 70.32 km to the northwest. The precipitation barycenter in May moves the smallest distance. Compared to the barycenter in April, the precipitation barycenter moves 8.17 km to the northeast. We observed
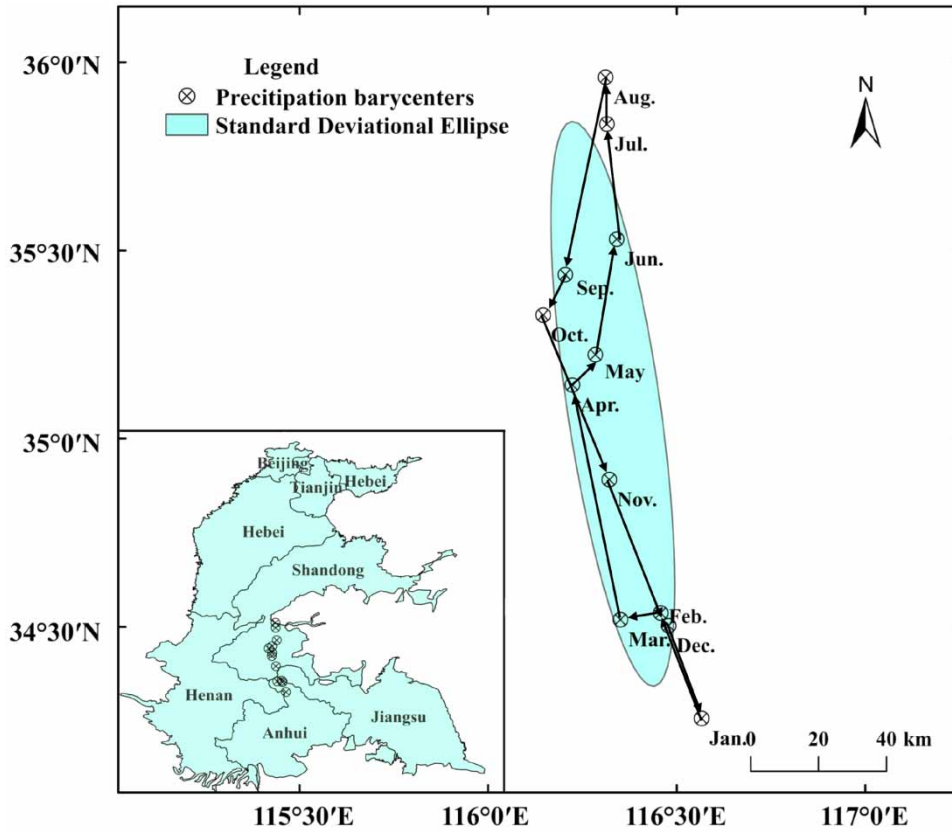
Figure 2 | Migration track of monthly precipitation barycenter on the '3H' Plain.

Table 1 | Movement direction and distance of monthly precipitation barycenter on the '3H' plain

Time	Precipitation barycenter (°)		Movement direction	Movement distance (km)
	Longitude	Latitude		
January	116.57	34.26	Southeast	28.49
February	116.46	34.54	Northwest	32.63
March	116.35	34.52	Southwest	9.98
April	116.22	35.14	Northwest	70.32
May	116.23	35.22	Northeast	8.17
June	116.34	35.53	Northeast	35.89
July	116.32	35.84	Northwest	34.06
August	116.31	35.96	Northwest	13.82
September	116.23	35.38	Southwest	64.41
October	116.15	35.33	Southwest	9.99
November	116.32	34.89	Southeast	51.26
December	116.48	34.50	Southeast	45.45

distinct movements of precipitation barycenters across months. The precipitation barycenters in February, April, July, and August move to the northwest. The precipitation barycenters for the three consecutive months of November, December, and January move to the southeast. The precipitation barycenters in March, September, and October move to the southwest.

By the season, the movement direction of the precipitation barycenter varies greatly in the four seasons. In spring (March–May), the movement direction of the precipitation barycenter changes considerably; there is no main direction, and the cumulative movement distance is 88.47 km. In summer (June–August), the precipitation barycenter mainly moves 83.77 km to the northwest, and the cumulative movement distance is the smallest. In autumn (September–November), the precipitation barycenter mainly moves 125.66 km to the southwest, and the cumulative movement distance is the largest. In winter (December–February), the precipitation barycenter mainly moves to the southeast, with a cumulative distance of 106.57 km. The trajectory of the monthly precipitation barycenter is generally '8'-shaped. In the rainy season (May–October), the precipitation barycenters are in the upper part of the '8'-shaped and are relatively concentrated, moving 166.34 km cumulatively. In the dry season (November–April), the precipitation barycenters are in the lower part of the '8'-shaped, and the distribution of the precipitation barycenters is relatively scattered, with a cumulative movement of 238.13 km. The above-mentioned migration pattern of the monthly precipitation barycenter is closely related to the precipitation amounts at the stations and their latitude and longitude positions. The precipitation on the '3H' Plain is primarily affected by the monsoon circulation, and the intensity of the influence of the monsoon circulation also plays an important role in the regional precipitation distribution (Zhang et al. 2020). The rainy season and the dry season are located at the upper and lower parts of the '8'-shaped, respectively. The northern part of the '3H' Plain has more rain in the rainy season and less rain in the dry season, which is prone to droughts and floods. Therefore, Beijing, Tianjin, and Hebei should strengthen the monitoring and early warning of drought and flood disasters. In the rainy season, preventive technical advice can be formulated to clear the gullies in advance to prevent large-scale waterlogging. In the dry season, artificial rainfall can be carried out to ensure agricultural production.

To further analyze the direction and dispersion of the monthly precipitation barycenters on the '3H' Plain, we created a first-level standard deviation ellipse for 12 precipitation barycenters. The direction of the standard deviation ellipse is 15.1° west by north. The major axis of the ellipse is located in the northwest-southeast direction. The minor axis of the ellipse is oriented in the southwest-northeast direction, and the oblateness is 0.86. These results show that the monthly precipitation barycenters are less dispersed in the southwest-northeast direction than in the northwest-southeast direction, and the distribution of monthly precipitation barycenters is apparent.

3.2. Distribution characteristics of interannual and interdecadal precipitation barycenters

To analyze the distribution and transfer of the precipitation barycenter on the '3H' Plain from 1960 to 2019, the latitude and longitude coordinates of precipitation barycenters were calculated with the annual precipitation as the weight. We drew a map of the migration track of precipitation barycenter from 1960 to 2019 (Figure 3). Figure 3 shows that the 60 interannual precipitation barycenters are distributed in Jining city and Tai'an city, Shandong Province. To quantitatively analyze the direction trend and clustering of the precipitation barycenters, we created a first-order standard deviation ellipse with 60 precipitation barycenters. The direction of the standard deviation ellipse is 1.0° west by north, and the oblateness of the ellipse is 0.68. It shows that the interannual precipitation barycenters on the '3H' Plain are distributed in the south-north direction. The average annual precipitation is more in the south and less in the north on the '3H' Plain. The average annual precipitation in the southern region exceeds 950 mm (Yi et al. 2017), and the weight of precipitation is higher. In addition, the '3H' Plain has a large latitude span and is affected by the East Asian summer monsoon. The above causes the spatial distribution pattern of the interannual precipitation barycenters to show a north-south direction. We analyzed the changes in the longitude and latitude coordinates of the interannual precipitation barycenters on the '3H' Plain in the past 60 years (Figure 4) and verified the significant changes by the Mann–Kendall method (Jia et al. 2018). The results show that the longitude and latitude coordinates of the interannual precipitation barycenters on the '3H' Plain show a decreasing trend from 1960 to 2019, but none of them pass the 90% significance test of reliability. Therefore, the interannual precipitation barycenter on the '3H' Plain has moved to the southwest in the past 60 years, but the overall trend is not obvious. The concept of the center of gravity determines that the distribution of the precipitation barycenter will tend to the area with more precipitation. It also verifies the conclusion that the spatial distribution of precipitation is increased in the southwest and decreased in the northeast on the '3H' Plain (Tian et al. 2019). The precipitation barycenter on the '3H' Plain moves to the southwest. It may have exacerbated the drought and water shortage in Beijing, Tianjin, and Hebei province, and increased the water supply pressure on the South to North Water Diversion Project.

We used the center-of-gravity model to calculate the precipitation barycenter in the 1960s, 1970s, 1980s, 1990s, 2000s, and 2010s. The six decadal precipitation barycenter distributions and movement tracks are shown in Figure 5. The changes in the precipitation barycenter in the six different decadal periods are not particularly significant, and all are located in western
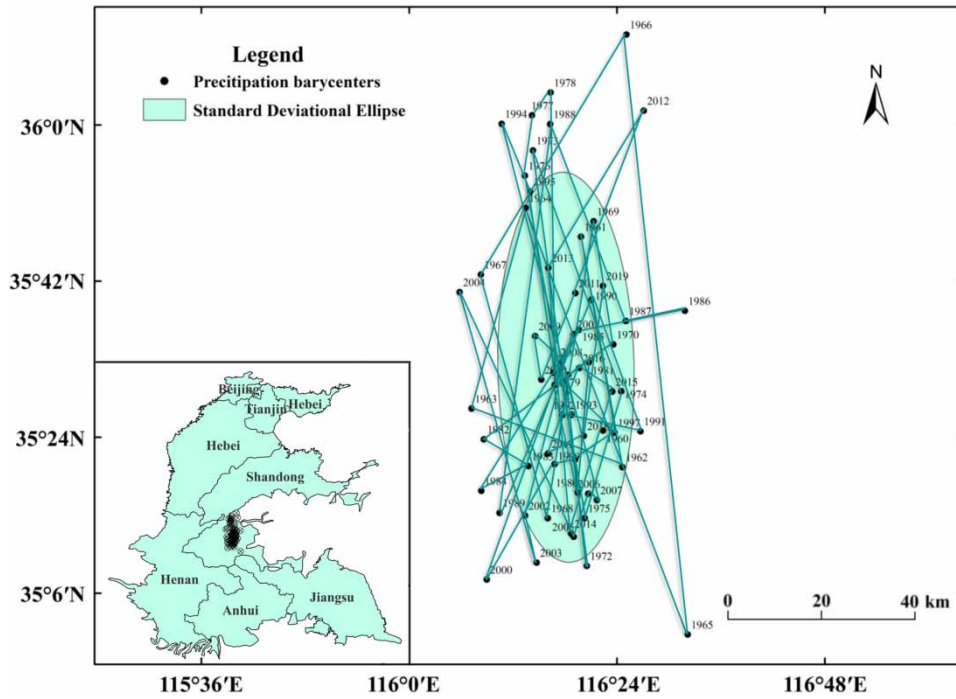
Figure 3 | Migration track of precipitation barycenter on the '3H' Plain from 1960 to 2019.
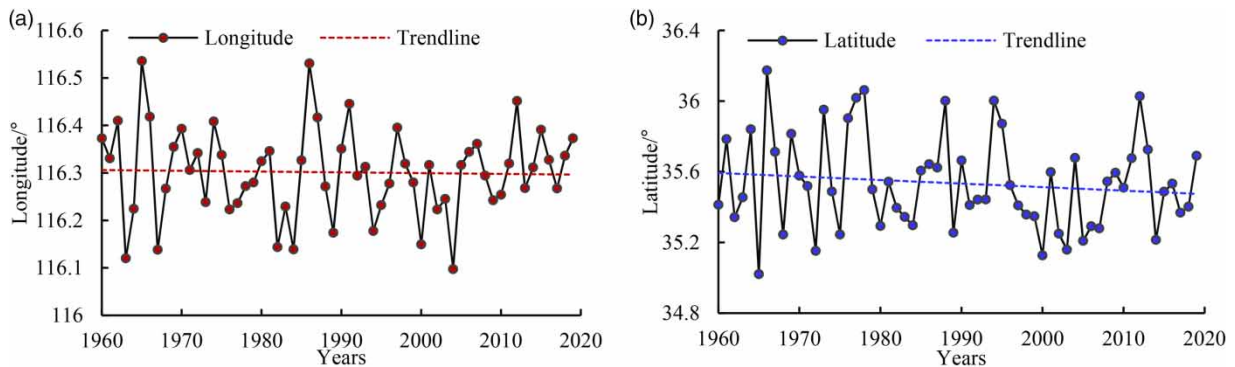

Figure 4 | Changes in the longitude (a) and latitude (b) coordinates of the precipitation barycenters from 1960 to 2019.

Jining city, Shandong Province. The positions of the precipitation barycenter in the 1960s and 1970s are close, and the precipitation barycenter moves only 5.53 km to the northwest. From the 1970s to the 1980s, the precipitation barycenter moves 16.46 km to the southwest. The precipitation barycenter moves 7.4 km to the northeast from the 1980s to the 1990s. Compared with the other five decadal locations, the precipitation barycenter in the 2000s shifts the most. During this period, the '3H' Plain has more precipitation, with an average annual precipitation of 692 mm. The large shift in the precipitation barycenter to the south indicates that the increase in precipitation in the northern part of the '3H' Plain is smaller than that in the southern part. From the 2000s to the 2010s, the precipitation barycenter moves 23.5 km to the northeast, which is the longest distance in the six decades.

The distribution and shift of the precipitation barycenter on the '3H' Plain are mainly affected by geographic location, topographic conditions, and atmospheric circulation. The geographic location and topographic conditions can be considered constant factors, but there are interdecadal variations in atmospheric circulation (Zhang *et al.* 2003). Therefore, the geographic location determines the average position of the precipitation barycenter on the '3H' Plain (Zhong 2020). The interaction between topographic conditions and atmospheric circulation promotes the migration of precipitation barycenter
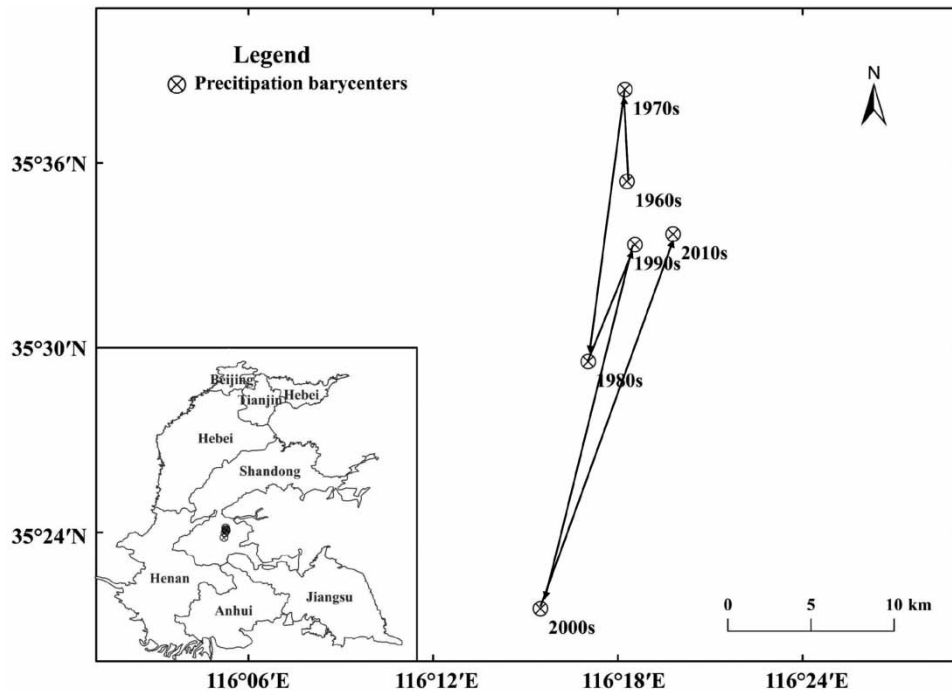
Figure 5 | Migration track of interdecadal precipitation barycenter on the '3H' Plain.

on the '3H' Plain to a certain regularity. As the signal with the strongest interaction between the ocean and the atmosphere in the world, ENSO is a key factor that causes the abnormal water vapor transport in the East Asian summer monsoon and the occurrence of droughts and floods (Zhang *et al.* 2013). ENSO affects the western Pacific subtropical high, which in turn affects the water vapor transport in the western Pacific, and thus has an effect on precipitation on the '3H' Plain (Mei *et al.* 2018). The subtropical high is northerly, and the summer monsoon is stronger (Susilo *et al.* 2013). The '3H' Plain has more precipitation, and vice versa. In addition, the distribution of precipitation barycenter tends to the regions with more precipitation, and precipitation barycenter on the '3H' Plain has been moving to the southwest in the past 60 years. Therefore, the precipitation barycenter may play a certain indicator role in the variation of the northwest monsoon and the East Asian monsoon.

3.3. Relationship between precipitation barycenter and the spatial distribution of station network

We analyzed the influence of the spatial distribution of the station network on the precipitation barycenter. In station network planning, the method of extracting stations is often used to study the rationality of station network layout (Lian *et al.* 2018). The precipitation barycenter calculated by 215 meteorological stations is called the approximate true value. Based on the principle of station extraction and considering the rationality of minimum density (we ensured that most cities on the '3H' Plain must select at least one site) and uniformity, 20 is determined to be the minimum number of stations in the station network, and 20, 30, 50, 70, 90, 110, 130, 150, 170, 190, and 200 stations are randomly selected 10 times to form 11 types of 110 station network distributions. The control area of each station is obtained by the Tyson polygon method. The uniformity index formula is introduced to calculate the distribution uniformity of each group of station networks (Cheng & Zhang 2017). The precipitation barycenter in each year under the spatial distribution of different station networks is taken as the theoretical value. Canonical correlation analysis can extract the typical variables and their canonical correlation coefficients that pass the significance test from the multidimensional variable group of the approximate true value and theoretical value of the annual precipitation barycenter. The canonical correlation coefficient reflects the closeness between the theoretical value and the approximate true value. The larger the canonical correlation coefficient, the closer the theoretical value of the precipitation barycenter is to the approximate true value.

Figure 6 is a scatter plot of 110 sets of station network uniformity and corresponding typical correlation coefficients under different station network densities. Figure 6(a) shows that the canonical correlation coefficients generally show an upward
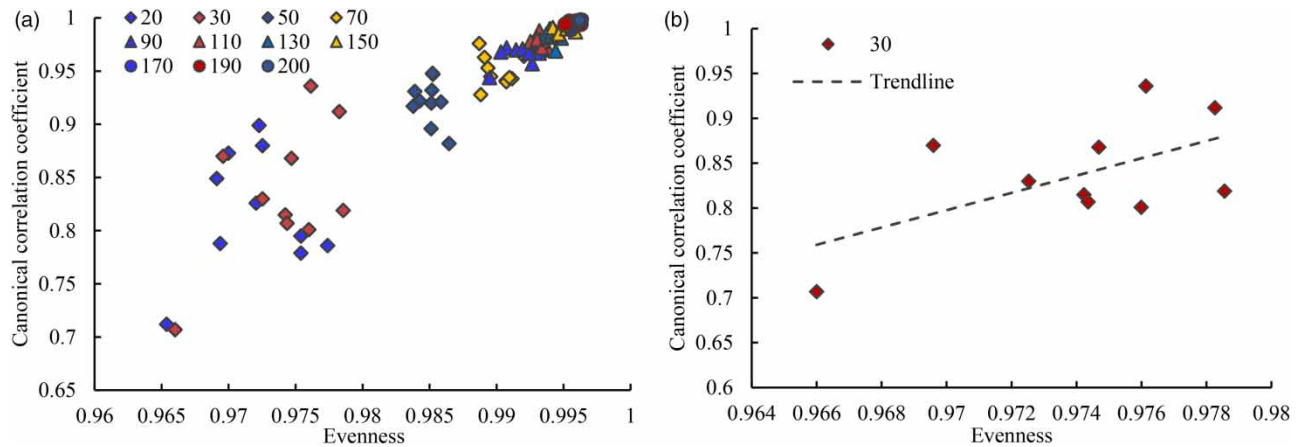
Figure 6 | Variations in canonical correlation coefficients under different meteorological station uniformities.

trend, as the uniformity of the station network increases. This indicates that the more uniform the station network is, the larger the canonical correlation coefficient and that the calculated precipitation barycenter is close to the approximate true value. In addition, when the station network density is low, the points in the graph are scattered, and the corresponding canonical correlation coefficient is small. When the density of the station network increases, the points in the figure are denser, and the corresponding canonical correlation coefficient is larger. When the station network density is large, the station network uniformity has less influence on the fluctuation range of the canonical correlation coefficient. When the station network density is low, the station network uniformity significantly influences the fluctuation range of the canonical correlation coefficient. To further analyze the influence of station network uniformity on the changes in the precipitation barycenter under the same station network density, we selected the distribution of 10 groups of station networks with 30 stations having a large uniformity change and analyzed the station network uniformity and its corresponding canonical correlation coefficient (Figure 6(b)). With increasing station network uniformity, the canonical correlation coefficient shows an overall upward trend. The station network uniformity under the same station network density has a positive correlation with the changes in the precipitation barycenter. To show more intuitively the influence of station network uniformity on the precipitation barycenter, we took the precipitation barycenter in 2019 as the research object and calculated the distance between the theoretical value of the precipitation barycenter and the approximate true value under different meteorological station uniformities. We drew a scatter diagram of the uniformity of 110 sets of station networks and their corresponding distances (Figure 7). Figure 7 shows that as the uniformity of the station network increases, the distance between the theoretical value of the precipitation barycenter and the approximate true value generally decreases. It shows that the more uniform the distribution of the station network, the closer the calculated precipitation barycenter is to the approximate true value.
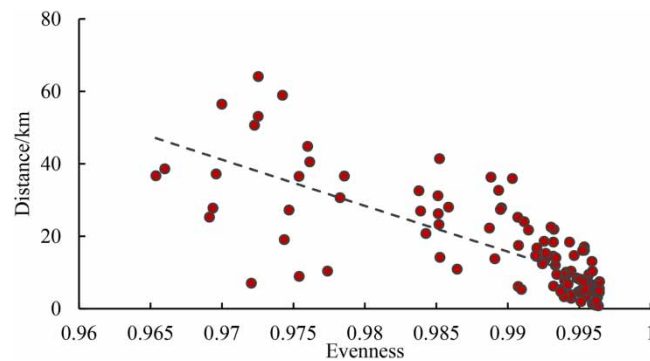

Figure 7 | Change of the distance between the theoretical value of the precipitation barycenter and the approximate true value under different meteorological station uniformities.
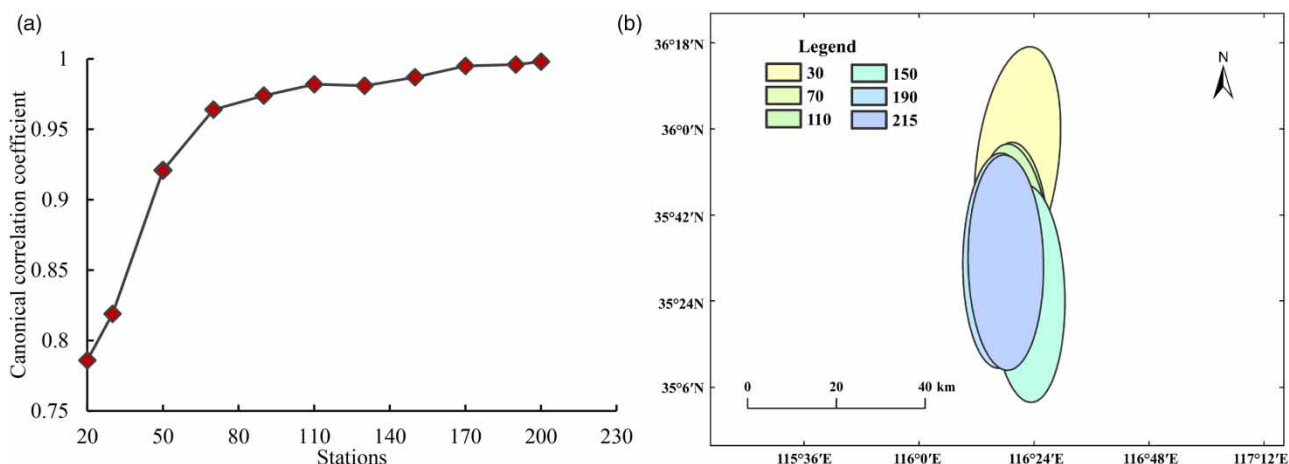
Figure 8 | Changes in canonical correlation coefficients (a) and standard deviation ellipse movement track (b) under different station network densities.

We selected 11 groups of station network distributions with different densities and similar station network uniformity and drew scatter plots of the number of stations and their corresponding canonical correlation coefficients (Figure 8(a)). We drew the first-level standard deviation ellipse of the precipitation barycenter under different station network densities (Figure 8(b)). Figure 8(a) shows that as the density of the station network increases, the canonical correlation coefficients show an upward trend. The increasing trend of the canonical correlation coefficient in the 20–70 site group is large, and the increase in the canonical correlation coefficient tends to flatten beyond the 70 site group. For a similar station network uniformity, the greater station network density is associated with larger corresponding canonical correlation coefficient and the calculated precipitation barycenter is closer to the approximate true value. When the station network density exceeds a certain range, the influence of station network density on the change in precipitation barycenter decreases. Figure 8(b) shows that the spatial gap for the precipitation barycenter in the same year under different station network densities can reach tens of kilometers, and the directivity and dispersion of the precipitation barycenter point group are somewhat different. The standard deviation ellipse of precipitation barycenters is mainly between 35°4′ and 36°17′N and 116°8′ and 116°28′. Besides, as the density of the station network increases, the standard deviation ellipse of the precipitation barycenter generally moves to the south. The direction of the ellipse fluctuates approximately 2° to the west of north, with a small fluctuation range, and the spatial distribution is generally oriented in the north-south direction. Affected by the East Asian monsoon, the annual average precipitation on the '3H' Plain is more in the south and less in the north, and the weight of precipitation in the south is higher. The southern part of the '3H' Plain occupies a larger area and has more meteorological stations. These may have caused the standard deviation ellipse of the precipitation barycenters to gradually move to the south.

4. CONCLUSION

1. The spatial distribution pattern of the monthly precipitation barycenters was oriented in the northwest-southeast direction with obvious directionality. The monthly precipitation barycenter generally followed an '8'-shaped movement track, and its upper and lower parts corresponded to the rainy and dry seasons, respectively.
2. The interannual precipitation barycenters on the '3H' Plain were distributed in Jining city and Tai'an city. The interannual precipitation barycenter had a trend of moving southwest, but the trend was not apparent. The position of the precipitation barycenter in the 2000s had the largest deviation compared to the other five decades.
3. The changes in the precipitation barycenter were correlated with the spatial distribution of the station network. If using a more uniform station network distribution and a greater station network density, the canonical correlation coefficient is larger, and the calculated precipitation barycenter is closer to the approximate true value. With similar station network uniformity, when the station network density exceeded a certain range, the influence of station network density on the changes in precipitation barycenter decreased.

DATA AVAILABILITY STATEMENT

All relevant data are included in the paper or its Supplementary Information.

REFERENCES

Barmpas, G., Kopsacheilis, A. & Politis, I. 2017 Small scale intervention in a major city center interchange: economic, environmental and sustainability analysis. *Transportation Research Procedia* **24**, 41–49.

Chen, S., Li, L., Li, J. & Liu, J. 2017 Analysis of the temporal and spatial variation characteristics of precipitation in the Lancang River basin over the past 55 years. *Journal of Geo-Information Science* **19** (03), 365–373.

Cheng, Z. & Zhang, X. 2017 Research on the relationship between the distribution of rainfall station and areal rainfall error. *China Rural Water and Hydropower* **10**, 174–178.

Fang, J., Guo, B., Zhang, Z., Chen, Z. & Wang, X. 2018 Temporal and spatial characteristics of precipitation extremes in the Huang-Huai-Hai Plain during 1960–2013. *Journal of Henan University (Natural Science)* **48** (02), 160–171.

Fu, Q., Li, T., Li, T. & Li, H. 2016 Temporal-spatial evolution patterns of the annual precipitation considering the climate change conditions in the Sanjiang Plain. *Journal of Water and Climate Change* **7** (1), 198–211.

Gao, Z. & Liu, J. 2006 The LUCC responses to climatic changes in china from 1980 to 2000. *Acta Geographica Sinica* **61** (08), 865–872. https://doi.org/10.1016/j.ijdrr.2020.101726.

Jia, Y., Zhang, B. & Ma, B. 2018 Daily SPEI reveals long-term change in drought characteristics in southwest china. *Chinese Geographical Science* **28** (4), 680–693.

Li, Y., Xie, Z., Qin, Y. & Zhou, S. 2018 Spatio-temporal variations in precipitation on the Huang-Huai-Hai Plain from 1963 to 2012. *Journal of Earth System Science* **127** (7), 101. https://doi.org/10.1007/s12040-018-0996.

Lian, M., Li, G., Dong, F. & Li, G. 2018 Study on appropriate precipitation station density based on station sampling method. *Water Resources and Power* **36** (06), 10–13.

Liu, B., Tao, H., Song, C., Guo, B. & Shi, Z. 2012 Study on annual variation of rainfall erosivity in southwest China using gravity center model. *Transactions of the Chinese Society of Agricultural Engineering* **28** (21), 113–120.

Luo, H., Li, C., Wei, J., Hou, C. & Ma, G. 2015 Accuracy validation of TRMM precipitation data in Shaxi River basin. *Journal of Subtropical Resources and Environment* **10** (04), 69–76.

Mei, C., Liu, J., Chen, M., Wang, H., Li, M. & Yu, Y. 2018 Multi-decadal spatial and temporal changes of extreme precipitation patterns in northern China (Jing-Jin-Ji district, 1960–2013). *Quaternary International* **476**, 1–13.

Qian, X. 2011 *Study on the Spatio-Temporal Evolution Law of Hydrological Cycle Elements on the Huai-bei Plain*. Yangzhou University, Yangzhou.

Robertson, M., Caithness, N. & Villet, M. 2001 A PCA-based modelling technique for predicting environmental suitability for organisms from presence records. *Diversity and Distributions* **7** (1), 15–27. https://doi.org/10.1046/j.1472-4642.2001.00094.x.

Rong, Y. & Luo, J. 2009 Evolution of climate change intensity in North China from 1901 to 2002. *Journal of Hohai University (Natural Sciences)* **37** (3), 276–280.

Sun, L., Hao, Z., Wang, J., Nistor, I. & Seidou, O. 2014 Assessment and correction of TMPA products 3B42RT and 3B42V6. *Journal of Hydraulic Engineering* **46** (10), 1135–1146.

Susilo, G., Yamamoto, k., Imai, T., Ishii, Y., Fukami, H. & Sekine, M. 2013 The effect of ENSO on rainfall characteristics in the tropical peatland areas of Central Kalimantan, Indonesia. *Hydrological Sciences Journal* **58** (3), 539–548. https://doi.org/10.1080/02626667. 2013.772298.

Tian, X., Li, B., Li, X., Li, T., Zhu, M. & Wang, L. 2019 Spatiotemporal variation of precipitable water and its influencing factors in the North China Plain during 1970–2012. *Journal of Liaocheng University (Natural Science Edition)* **32** (03), 81–88.

Wu, K., Wang, X., Xu, Y., Wang, G. & Wu, Y. 2017 New facts about evolution of spatial and temporal pattern of precipitation over Chinese mainland. *South-to-North Water Transfers and Water Science & Technology* **15** (03), 30–36.

Wu, X., Wang, P., Gong, Y. & Yang, J. 2019 Analysis of drought identification and spatio-temporal characteristics for summer corn in Huang-Huai-Hai Plain in year of 1961–2015. *Transactions of the Chinese Society of Agricultural Engineering* **35** (18), 189–199.

Yang, J., Mei, X., Huo, Z., Yan, C., Ju, H., Zhao, F. & Liu, Q. 2015 Water consumption in summer maize and winter wheat cropping system based on SEBAL model in Huang-Huai-Hai Plain China. *Journal of Integrative Agriculture* **14**, 2065–2076. https://doi.org/10.1016/S2095-3119(14)60951-5.

Yao, R., Xia, M., Sun, P., Wen, Q., Liu, G. & Liang, Y. 2021 Spatio-temporal distribution characteristics of meteorological drought and climate influence factors. *Acta Ecologica Sinica* **41** (01), 333–347.

Yi, J., Wu, S., Yang, Z., Yuan, J. & Yuan, Y. 2017 Precipitation variation in Huang-Huai-Hai region in the recent 50 years. *Yellow River* **39** (04), 11–16.

Yuan, Y., Yan, D., Yuan, Z., Yin, J. & Zhao, Z. 2019 Spatial distribution of precipitation in Huang-Huai-Hai River Basin between 1961 to 2016, China. *International Journal of Environmental Research and Public Health* **16** (18), 3404. https://doi.org/10.3390/ijerph16183404.

Yuan, J., Bian, Z., Yan, Q., Gu, Z. & Yu, H. 2020 An approach to the temporal and spatial characteristics of vegetation in the growing season in western China. *Remote Sensing* **12** (6), 945.

Zhang, Q., Tao, S. & Chen, L. 2003 The interannual variation of East Asian summer monsoon index and East Asian atmospheric circulation. *Acta Meteorologica Sinica* **61** (05), 559–568.

Zhang, X., Chen, S., Sun, H., Shao, L. & Wang, Y. 2011 Changes in evapotranspiration over irrigated winter wheat and maize in North China Plain over three decades. *Agricultural Water Management* **98**, 1097–1104. https://doi.org/10.1016/j.agwat.2011.02.003.

Zhang, Q., Li, J., Singh, V., Xu, C. & Deng, J. 2013 Influence of ENSO on precipitation in the East River basin, South China. *Journal of Geophysical Research: Atmospheres* **118** (5), 2207–2219.

Zhang, D., Yan, D., Wang, Y., Lu, F. & Wu, D. 2015 Changes in extreme precipitation in the Huang-Huai-Hai River basin of China during 1960–2010. *Theoretical and Applied Climatology* **120**, 195–209.

Zhang, P., Xu, X. & Wang, Y. 2020 Impacts of subgrid orographic drag on the summer monsoon circulation and precipitation in East Asia. *Journal of Geophysical Research: Atmospheres* **125** (13). https://doi.org/10.1029/2019JD032337.

Zhao, Z., Luo, Y., Yu, J., Luo, X. & Yang, Y. 2018 Analysis of precipitation variation characteristics and barycenter shift in Guizhou Plateau during 1960–2016. *Journal of Geo-Information Science* **20** (10), 1432–1442.

Zhong, S. 2020 Advances in the study of the influencing mechanism and forecast methods for orographic precipitation. *Plateau Meteorology* **39** (05), 1122–1132.

Zhuang, X., Yang, Z. & Cordes, D. 2020 A technical review of canonical correlation analysis for neuroscience applications. *Human Brain Mapping* **41** (13), 3807–3833.